ISSN 1062-8738, Bulletin of the Russian Academy of Sciences: Physics, 2022, Vol. 86, No. 7, pp. 841–845. © Allerton Press, Inc., 2022.
Russian Text © The Author(s), 2022, published in Izvestiya Rossiiskoi Akademii Nauk, Seriya Fizicheskaya, 2022, Vol. 86, No. 7, pp. 1013–1018.

Relationship between Thermal and Dynamic Radiation in a Spin-Injection THz Emitter

A. I. Panas[a], S. G. Chigarev[b, *], E. A. Vilkov[b], O. A. Byshevski-Konopko[b], D. L. Zagorskiy[c], and I. M. Doludenko[c]

[a] *Shokin ISTOK Research and Production Enterprise, Fryazino, 141190 Russia*
[b] *Kotelnikov Institute of Radio Engineering and Electronics, Russian Academy of Sciences, Fryazino Branch, Fryazino, 141190 Russia*
[c] *National Research Center "Crystallography and Photonics," Russian Academy of Sciences, Moscow, 119333 Russia*
**e-mail: chig50@mail.ru*

Received February 14, 2022; revised February 28, 2022; accepted March 23, 2022

Abstract—The operation of a spin-injection THz emitter is used to establish the possibility of competition between thermal and spin-injection (dynamic) radiation. It is shown experimentally that raising the intensity of dynamic radiation lowers that of thermal radiation. This is explained by the relationship between dynamic radiation and indirect interband spin-flip transitions accompanied by a change in momentum, and thus the absorption of phonons.

DOI: 10.3103/S1062873822070243

INTRODUCTION

Studying processes in such spintronics components as micro- and nano-heterostructures containing ferromagnetic (FM) and antiferromagnetic (AFM) metals (magnetic transitions) are of interest because of the many ways in which they can be used [1–3]. It was shown in [4–6] that THz radiation can be generated when a current flows through a magnetic FM–FM junction, due to the spin-polarization flux of free electrons and its separation between spin subbands, resulting in spin-flip electron transitions among them. In practical terms, this can be used as a basis for developing quantum generators with current pumping, which is of utmost importance in the THz range. Nowadays, THz emitters that use spin injection through the current in magnetic transitions [7–12] can be considered an option in using this mechanism.

In experimental studies of prototypes of operating spin-injection emitters, a signal is detected in the 7–30 THz range of frequencies, which partly overlaps with the maximum of thermal radiation of a body heated to ~100°C. Since a current of up to 1 A can flow through a spin-injection emitter in the operating regime of the device and heat it to such temperatures, thermal and dynamic radiation can be detected concurrently in the radiation spectrum. It is natural that the composition of the emitted power depends on the efficiency of the spin-injection emitter's operation. In some cases [9], dynamic radiation accounts for several percent of the total radiation power. If the source is more efficient, thermal radiation is virtually not detected [11].

Some suppression of thermal radiation in a spin-injection emitter's operation can be explained by the nature of dynamic radiation, which (as we noted in [7, 12]) is driven by both direct and indirect quantum transitions that require the absorption of photons. This means that in practice, heat is removed from the working body. The absorption of photons can therefore reduce the thermal effect of the electric current, which we believe can diminish the intensity of thermal radiation. This can result in competition between radiative processes that are of dynamic or thermal nature. However, this hypothesis requires additional detailed studies. Some results obtained in such studies are presented below.

EXPERIMENTAL OBSERVATION OF COMPETITION BETWEEN RADIATION MECHANISMS

Experimental observations were made on a most efficient spin-injection THz emitter based on a set of nanowires [13]. Measurements were made using a Vertex 80 V spectral analyzer manufactured by Bruker. Figure 1 shows the spectrum of a detected signal in the 10–25 μm range of wavelengths, measured at different amperages.

During the operation of the emitter, the stabilized voltage was raised from 0 to 11 V in steps of 1 V. When the voltage reached 11 V, the emitter's operation was

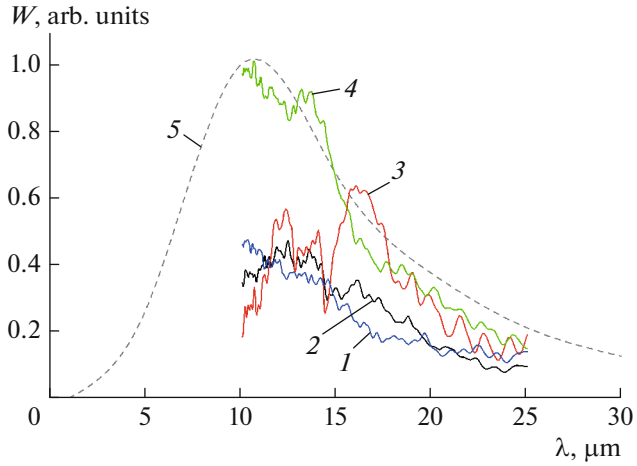

Fig. 1. Spectrum of detected signal at different amperages: (*1*) $I = 10$ mA, (*2*) $I = 50$ mA, (*3*) $I = 85$ mA, (*4*) $I = 14$ mA (after emitter operation), (*5*) calculated Planck curve.

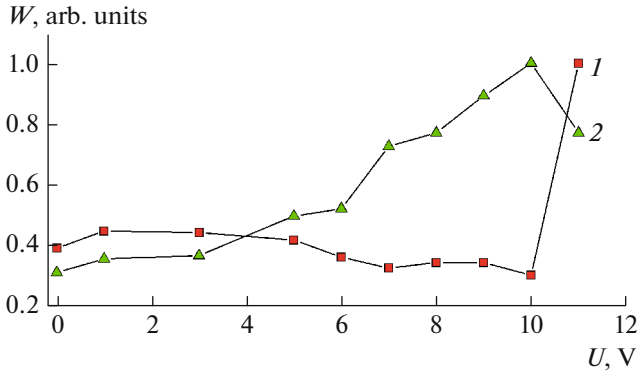

Fig. 2. Radiation intensity (in arbitrary units) as a function of voltage on the emitter for various wavelengths: (*1*) $\lambda = 10$ μm (maximum of the Planck curve for a "hot" body); (*2*) $\lambda = 16$ μm (maximum of dynamic radiation).

interrupted as a result of a surge in its resistance, due to irreversible structural changes in the nanowires. The temperature of the emitter's surface was ~80°C. The results presented in Fig. 1 show that the behavior of spectral curves was of two different types. For amperages below ~53 mA, the intensity of the signal in the considered range of wavelengths rose monotonically to the maximum value at $\lambda \sim 10$ μm. Such behavior of the spectrum corresponds to that of the Planck curve for "hot" body radiation. For amperages in the range of 53 mA (7 V) to 85 mA (10 V), radiation power at a level of 3-dB was observed in the 15–17 μm range of wavelengths. The intensity of radiation at wavelengths that corresponded to the maximum of thermal radiation on the Planck curve ($\lambda \sim 10$ μm) was lower than at $\lambda \sim 16$ μm (see curve *3* in Fig. 1). The threshold value of the current needed for the peak power concentration to be reached led to conclusions about the non-thermal and dynamic nature of the radiation in this range of λ. However, the radiation maximum was observed at $\lambda \sim 10$ μm when there was no dynamic radiation (curves *1*, *2*, and *4*). Dynamic radiation (an amperage of 14 mA, which was lower than the initial value) vanished after the emitter's operation ceased at a voltage of 11 V, and the plot of the "hot" emitter spectrum (curve *4*) resembled the one calculated for Planck's thermal radiation (dashed curve *5* in Fig. 1).

The competition between the radiation mechanisms is seen more easily in Fig. 2, which displays the intensity of radiation detected at two different wavelengths as a function of voltage. Curve *1* corresponds to the change in the intensity of the radiation detected at the wavelength that corresponds to the maximum of thermal radiation, which coincides with the maximum of the Planck curve ($\lambda = 10$ μm). Curve *2* corresponds to the maximum of dynamic radiation ($\lambda = 16$ μm).

Voltage is used here as the variable because its value was stabilized at each step. The current could vary within a narrow range, due to some heating of the array of nanowires. Because of structural changes in the nanowires, their resistance surged at a voltage of 11 V. The amperage dipped to 14 mA, but the voltage remained unchanged. Using voltage as a variable parameter therefore allowed us to obtain voltage dependences of radiation intensity that were fairly monotonic.

Analyzing the changes in the curves of the intensities of thermal (curve *1*) and dynamic (curve *2*) radiation, we see the intensity of radiation grew for both curves when the emitter was activated ($U = 1$ V), which can be explained by the dominance of the thermal component radiated at both wavelengths. However, the intensity of thermal radiation at $\lambda = 10$ μm starts to fall considerably as the voltage (working current) rises from a value of around 3 V, while that of dynamic radiation grows. Two segments where dynamic radiation grows along with voltage are observed. The first and flatter segment ranges from $U = 3$ to 6 V, and more rapid growth of radiation power is observed when $U = 6$ V. We may therefore assume the existence of two different mechanisms that generate dynamic radiation via spin injection and differ by the efficiency of the emitter's operation. This is confirmed by comparimg the results presented in both figures. While the intensity of dynamic radiation is low in the 3–6 V range of voltages and thermal radiation dominates (curve *2* in Fig. 1), the intensity of dynamic radiation grows rapidly and exceeds that of thermal radiation at voltages above 6 V (current 55 mA) (curve *3* in Fig. 1). We believe this surge of dynamic radiation is associated with the enhanced absorption of phonons. However, this phenomenon requires special and detailed investigation. Dynamic radiation vanishes when the voltage reaches 11 V (the current is 14 mA lower than the initial value). The thermal radiation grows in a stepwise

manner, and the curve describing it resembles that of Plank's thermal radiation. The behavior of each curve mirrors that of the other, with an opposite sign. The thermal radiation is reduced as the dynamic radiation grows, and vice versa. It is this behavior of the curves that led us to hypothesize there was competition between the thermal and dynamic radiation.

EXPLAINING THE OBSERVED EFFECT

To explain the competition between thermal and dynamic radiation, we must consider how radiation is generated when current flows through the magnetic junction of a spin-injection emitter using the temperature field formalism. In our case, the magnetic junction can be represented as a thermodynamic system with two degrees of freedom. One is associated with the heat of the emitter and is described in quantitative terms by a relation derived by transforming the Planck equation:

$$T_p = \frac{h\nu_p}{k_B} \frac{1}{\ln\left(A\frac{h\nu_p}{u} + 1\right)}. \quad (1)$$

Here, h is the Planck constant, ν_p is the frequency of thermal radiation, k_B is the Boltzmann constant, $A = 8\pi\nu^2/c^2$, and u is the emissivity of an absolutely black body. Another degree of freedom associated with the partial nonuniformity of the spin state of the magnetic system is determined by the equation for the spin temperature [7]:

$$T_s = \frac{h\nu_s}{k_B} \frac{1}{\ln\left(\frac{1-P}{1+P}\right)}. \quad (2)$$

Here, T_s is the spin temperature, ν_s is the frequency determined by the spin nonuniformity of the system, and P is the spin polarization.

Comparing Eqs. (1) and (2), we see they are qualitatively identical. In both cases, temperature is proportional to emitted energy $h\nu$ and inversely proportional to emissivity, which is determined in Eqs. (1) and (2) by the argument of natural logarithm. In the first case, it is associated with emissivity u of the emitter heated by the current; in the second, with the emergence of spin imbalance in the magnetic junction upon spin injection by the current, which is governed by spin polarization P. In both cases, the source of energy for the changing temperature is the current that flows through the magnetic junction. Since the source of energy for the considered processes is the same suggests a possible relationship between them for radiation in the same range of frequencies, $\nu_p \sim \nu_s$.

Let us now consider in more detail how spin polarization can be associated with the heat of the emitter. Since our theoretical analysis of the process was based on assumptions that greatly simplify the considered spin injection, the conclusions presented below should be considered a qualitative estimate of the actual process.

It is known [6] that if a current crosses interfaces between layers of a magnetic junction, spin concentration P in the working layer changes at spin relaxation distance $l = \sqrt{D\tau} \sim 30$ nm from the interface. This change is described by the equation

$$\frac{d^2P}{dx^2} - \frac{j}{j_D l}\frac{dP}{dx} - \frac{P - P_2}{l^2} = 0. \quad (3)$$

Equation (3) was derived with allowance for conservation of the electric charge, $\vec{\nabla}\cdot\vec{j} = 0$, [7] and by assuming charge carriers in both spin subbands have the same values of mobility $\mu_- = \mu_+ = \mu$ and coefficients of diffusion $D_- = D_+ = D$. Here and below, τ is the period of spin relaxation, $j_D = enD/l = enl/\tau$ is the density of the current of electron diffusion, n is the density of electrons in metal, P_2 is the equilibrium spin polarization of the working area (the ferromagnetic material into which spin-polarized electrons are injected), and P is the non-equilibrium spin polarization of the working area.

The process described by Eq. (3) is shown schematically in Fig. 3 for layers magnetized in opposite directions, a situation studied in [13]. That work showed that when an external source of voltage V is applied to a magnetic junction, spin-polarized current I flows through it and generates radiation. Figure 3 shows three areas. Area I corresponds to a ferromagnetic injector in which electrons are distributed among spin energy subbands. The electrons are in a state of spin equilibrium where the spins of most are oriented parallel to the injector's magnetization (major electrons), while those of the remainder are oriented antiparallel (minor electrons). The subbands have a common equilibrium Fermi level, and the subband bottoms are separated by a value proportional to energy of exchange $I_1 = \mu_B\alpha_{sd1}M_1$. Area II is the working area (FM or AFM), the magnetic properties of which differ from those of the injector. Electrons in this area are in a nonequilibrium spin state because, due to the opposite orientation of layer magnetization and conservation of the system's spin state, major injector electrons become minor electrons in the working area, and *vice versa*. Fermi quasi-levels $\varepsilon_{F\pm}$ emerge, and the subband bottom splitting varies in proportion to the change in energy of exchange I_2. Spin-flip transitions of nonequilibrium electrons between bands occur under the effect of external factors, due possibly to the emission of energy quanta. Area III is the area where an equilibrium spin state is established after the relaxation of nonequilibrium spins.

A detailed solution to Eq. (3) is presented in [8]. The obtained equation determines the deviation of

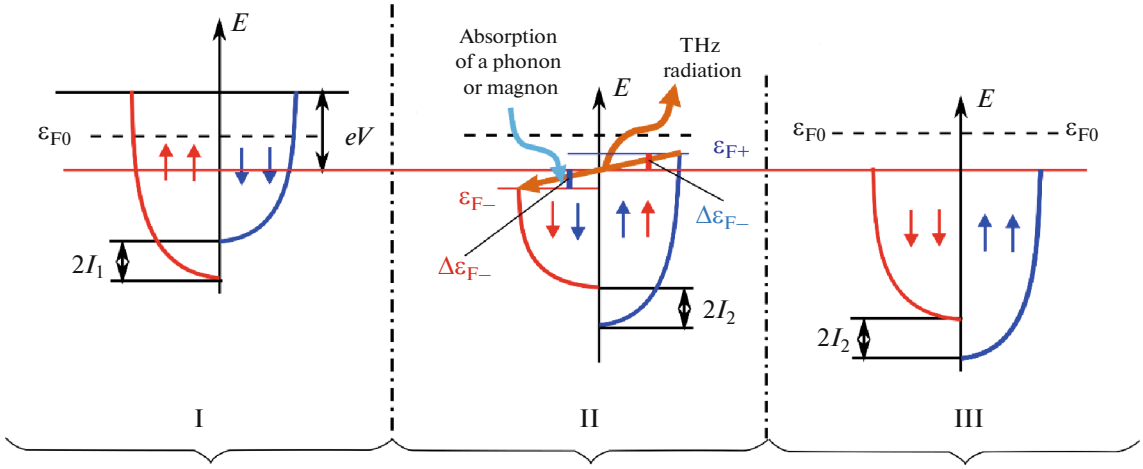

Fig. 3. Diagram of electron energy bands and Fermi quasi-levels: (I) first ferromagnetic; (II) for nonequilibrium electrons in the second ferromagnetic; (III) equilibrium electrons in the second ferromagnetic outside the injection region.

spin polarization from equilibrium value $\Delta P = P - P_2$, where P for $j/j_D \ll 1$ can be written in the form

$$P(x) = P_2 + \frac{P_1 \cos\varphi - P_2}{j_D} j \exp(-x/l). \qquad (4)$$

Here, P_1 is the equilibrium spin polarization of the injector, φ is the angle between the directions of layer magnetization, j is the current density, and x is the coordinate of current propagation.

This equation describes the energy process in the magnetic junction as [8]:

$$\begin{aligned} h\nu &= (\Delta\varepsilon_{F+} + \Delta\varepsilon_{F-}) \\ &= (\varepsilon_{F+} - \varepsilon_{0F+}) - (\varepsilon_{F-} - \varepsilon_{0F-}) \\ &= \frac{\hbar^2}{2m}(3\pi^2 n)^{2/3}\left(\left(\frac{1-P}{2}\right)^{2/3} - \left(\frac{1+P}{2}\right)^{2/3}\right. \\ &\left. - \left(\left(\frac{1-P_2}{2}\right)^{2/3} - \left(\frac{1+P_2}{2}\right)^{2/3}\right)\right) \\ &= (\varepsilon_{F+} - \varepsilon_{F-}) + 2I_2. \end{aligned} \qquad (5)$$

According to Eq. (5), the emitter's spin-injection mechanism of radiation in the parabolic approximation $\varepsilon = p^2/2m$ we adopted is governed by two qualitatively different processes. Some electrons change their energy while preserving their momentum. The spin-flip transition of electrons between bands is associated with energy of exchange $2I_2$, indicating these transitions are direct quantum transitions. Other electrons vary their energy in the $(\varepsilon_{F+} - \varepsilon_{F-})$ range with a change in momentum, indicating such transitions are indirect quantum transitions that extract energy from the environment with the absorption of phonons or magnons. This process can partially absorb heat, as is shown in Figs. 1 and 2.

CONCLUSIONS

Our study of the spin-injection emitter described above showed that its radiation spectrum contained two components, one of which was associated with the emitter being heated by the electric current (thermal radiation) and another component of non-thermal nature that we associate with spin injection by the current (dynamic radiation). Since the dynamic radiation is partly determined by indirect quantum transitions that require the absorption of a third particle (a phonon), it can reduce the heating of the emitter by the current. This can lower the intensity of thermal radiation in spin-injector operation, which can be interpreted as competition between the two types of radiation.

FUNDING

This work was supported by the Russian Foundation for Basic Research, project nos. 19-29-03015-mk and 20-07-00349-a. It was performed as part of government contracts with National Research Center "Crystallography and Photonics" and the Kotelnikov Institute of Radio Engineering and Electronics.

CONFLICT OF INTEREST

The authors declare that they have no conflicts of interest.

REFERENCES

1. Baltz, V., Manchon, A., Tsoi, M., et al., *Rev. Mod. Phys.*, 2018, vol. 90, no. 1, 015005.
2. Dhillon, S.S., Vitiello, M.S., Linfield, E.H., et al., *J. Phys. D: Appl. Phys.*, 2017, vol. 50, no. 4, 043001.
3. Hellman, F., Hoffmann, A., Tserkovnyak, Y., et al., *Rev. Mod. Phys.*, 2017, vol. 89, no. 2, 025006.

4. Kadigrobov, A., Ivanov, Z., Claeson, T., et al., *Europhys. Lett.*, 2004, vol. 67, no. 6, p. 948.

5. Kadigrobov, A.M., Shekhter, R.I., and Jonson, M., *Low Temp. Phys.*, 2012, vol. 38, no. 12, p. 1133.

6. Kadigrobov, A.M., Shekhter, R.I., Kulinich, S.I., et al., *New J. Phys.*, 2011, vol. 13, no. 2, 023007.

7. Gulyaev, Yu.V., Zil'berman, P.E., Epshtein, E.M., and Elliott, R.J., *J. Commun. Technol. Electron.*, 2003, vol. 48, no. 9, p. 942.

8. Gulyaev, Yu.V., Zil'berman, P.E., Krikunov, A.I., et al., *JETP Lett.*, 2007, vol. 85, no. 3, p. 160.

9. Gulayev, Yu.V., Zilberman, P.E., Chigarev, S.G., and Epshtein, E.M., *J. Commun. Technol. Electron.*, 2010, vol. 55, no. 10, p. 1132.

10. Chigarev, S.G., Malikov, I.V., and Mikhailov, G.M., *J. Commun. Technol. Electron.*, 2013, vol. 58, no. 3, p. 238.

11. Vilkov, E.A., Dyuzhikov, I.N., Zaitsev-Zotov, S.V., et al., *J. Commun. Technol. Electron.*, 2018, vol. 63, no. 9, p. 1015.

12. Gulayev, Yu.V., Zil'berman, P.E., and Chigarev, S.G., *J. Commun. Technol. Electron.*, 2015, vol. 60, no. 5, p. 411.

13. Vilkov, E.A., Mikhailov, G.M., Chigarev, S.G., et al., *J. Commun. Technol. Electron.*, 2016, vol. 61, no. 9, p. 995.

14. Gulyaev, Yu.V., Chigarev, S.G., Panas, A.I., et al., *Tech. Phys. Lett.*, 2019, vol. 45, no. 3, p. 271.

Translated by M. Shmatikov